

Grid-Free Vortex Method for Particle-Laden Gas Flow

T. Uchiyama¹

Abstract: This study proposes a three-dimensional grid-free method to simulate particle-laden gas flows. It is based on a vortex method. The flow region is not resolved into computational grids, but the gas vorticity field is discretized by vortex elements. The behavior of the vortex element and the particle motion are simultaneously calculated by using the Lagrangian approach. Eight cubic cells are locally allocated around each particle to compute the effect of the particle motion on the gas flow. In each cell, the change in the vorticity due to the particle is calculated, and it is considered by generating a vortex element or changing the strength of the existing vortex elements. This study also applies the grid-free method to simulate a free fall of small spherical solid particles. The particles, initially arranged within a spherical region in an unbounded quiescent air, are made to fall, and their fall induces the air flow around them. The particles are accelerated by the induced downward air flow just after the commencement of their fall. After the acceleration, they are whirled up by a vortex ring produced around the downward air flow. These results are in good agreement with the existing ones, demonstrating the validity of the proposed grid-free method.

Keywords: Gas-particle two-phase flow, Lagrangian calculation, Vortex method

Notations

C_D : drag coefficient for particle

d : particle diameter

D : diameter of particle-cluster at initial condition

F_D : force exerted by particle acting on gas-phase per unit volume

f_D : drag force acting on particle

g : gravitational acceleration

L : side length of cubic cell around particle

¹ Nagoya University, Nagoya, JAPAN

- p : pressure
 t : time
 t^* : nondimensional time $=u_t t/D$
 u : velocity
 u_t : terminal velocity of particle
 \bar{u}_p : averaged velocity of falling particles
 v_p : particle velocity relative to gas $=u_p - u_g$
 V : volume of grid and cell
 x, y, z : orthogonal coordinates
 Δt : time increment
 γ : strength of vortex element
 θ : angle between f_D and x -axis
 ν : kinematic viscosity
 ρ : density
 σ : core radius of vortex element
 φ : angle between f_D and z -axis
 ω : vorticity $=\nabla \times u_g$
- Subscript
- g : gas
 p : particle

1 Introduction

For numerical simulations in a wide variety of continuum mechanics, the development of a method that needs no computational grids is earnestly demanded. Such grid-free method is especially effective in a simulation handling a computational domain with complicated geometries. Because the simulation takes much more work to resolve the domain into the grids. A vortex method attracts much attention as one of the grid-free methods simulating an incompressible flow (Winckelmans, 2004; Cottet and Koumoutsakos, 2000). It discretizes the vorticity field into vortex elements and calculates the time evolution of the flow by tracing the motion of the vortex element by using the Lagrangian approach. A number of studies on the vortex method for single-phase flow simulation have been conducted. It is demon-

strated that the vortex method is usefully applicable to solve a wide class of flow problems from low to high Reynolds numbers.

Gas flows loaded with small solid particles are observed in many industrial applications, such as chemical plants and energy conversion systems. Various simulation methods have thus far been proposed (Crowe et al., 1992). Lagrangian approach is applied to simulate the particle motion. Eulerian methods employing computational grids are frequently used to simulate the gas flow in the similar way as the single-phase flow simulation. Therefore the simulation methods are of a Lagrangian-Eulerian type. To extend the applicability of vortex method, the author (Uchiyama and Naruse, 2001; Uchiyama and Naruse, 2004; Uchiyama and Fukase, 2005) proposed vortex methods for gas-particle two-phase flow. The vortex methods discretize the vorticity field into vortex elements, and calculate the behavior of the vortex element as well as the particle motion by the Lagrangian approach. The effect of the particle on the gas flow is considered through the variation for the strength of vortex element, which is caused by the change in the circulation due to the particle motion. Since the computational grids resolving the entire flow field are employed to calculate the change in the circulation, one of the advantages of a vortex method, namely the grid-free technique, was not fully exhibited.

This study proposes a grid-free method, which is based on a vortex method, for gas-particle two-phase flow. The method does not resolve the entire flow field into computational grids. As the simulation for a flow field having complicated geometries needs much work to resolve the field into the grids, one can accelerate the simulation efficiency by the method. Eight cubic cells are allocated around each particle to compute the effect of the particle on the gas flow. In each cell, the change in the vorticity due to the particle motion is calculated, and it is considered by generating a vortex element or changing the strength of the existing vortex elements. The proposed grid-free method is also applied to simulate a free fall of small spherical solid particles in air to demonstrate the validity. The particles, initially arranged within a spherical region in an unbounded air, are made to fall, and their fall induces the air flow around them, resulting in a gas-particle two-phase flow. The particles are accelerated by the induced downward air flow just after the commencement of their fall. After the acceleration, they are whirled up by a vortex ring produced around the downward air flow. These interactions between the particle motion and the air flow are favorably compared with the existing measured and simulated results, demonstrating the validity of the proposed grid-free method.

2 Basic Equations

2.1 Assumptions

The following assumptions are employed in the simulation.

- (1) The gas-phase is incompressible.
- (2) The particle has a spherical shape with uniform diameter.
- (3) The collision between the particles is negligible.
- (4) The particle Reynolds number is less than 300, and accordingly no vortices are shed from the particle.

2.2 Governing equations for gas and particle

The conservation equations for the mass and momentum of the gas-phase are expressed as follows under the assumption (1):

$$\nabla \cdot u_g = 0 \quad (1)$$

$$\frac{\partial u_g}{\partial t} + (u_g \cdot \nabla) u_g = -\frac{1}{\rho_g} \nabla p + \nu \nabla^2 u_g - \frac{1}{\rho_g} F_D \quad (2)$$

where F_D is the force exerted by the particle acting on the gas-phase per unit volume.

It is postulated the particle density is much larger than the gas. The dominant forces on the particle are the drag and gravitational forces, while the virtual mass force, the Basset force, and the pressure gradient force are negligible. Consequently, the equation of motion for a particle (mass m , density ρ_p) is written as:

$$m \frac{du_p}{dt} = f_D + (1 - \rho_g/\rho_p) mg \quad (3)$$

where the drag force f_D is given by the following:

$$f_D = (\pi d^2 \rho_g / 8) C_D |u_g - u_p| (u_g - u_p) \quad (4)$$

Here, d is the particle diameter, and the drag coefficient C_D is estimated as (Schiller and Naumann, 1933):

$$C_D = (24/\text{Re}_p)(1 + 0.15\text{Re}_p^{0.687}) \quad (5)$$

where $\text{Re}_p = d|u_g - u_p|/\nu$.

For the simultaneous calculations of Eqs. (1)~(3), a vortex method is used to solve Eqs. (1) and (2), and the Lagrangian approach is applied to Eq. (3).

2.3 Discretization of gas vorticity field by vortex element

Taking the curl of Eq. (2) and substituting Eq. (1) into the resultant equation, the vorticity equation for the gas is derived:

$$\frac{\partial \omega}{\partial t} + (u_g \cdot \nabla) \omega = (\omega \cdot \nabla) u_g + \nu \nabla^2 \omega - \frac{1}{\rho_g} \nabla \times F_D \quad (6)$$

where ω is the vorticity.

The gas velocity u_g at x is given by the Biot-Savart equation:

$$u_g(x) = -\frac{1}{4\pi} \int \frac{(x-x') \times \omega(x')}{|x-x'|^3} dV(x') + u_{g0} \quad (7)$$

where u_{g0} stands for the velocity of the potential flow or the uniform flow.

The gas vorticity field is discretized by vortex elements. Various models for the vortex element have been proposed. This study employs a blob model for single-phase flow simulation (Winckelmans and Leonard, 1993). The vortex element has a cylindrical shape, while the vorticity distribution is spherical with a finite core radius. When the vortex element α at x^α is presumed to have the core radius σ_α , the vorticity at x induced by the element is expressed as:

$$\omega^\alpha(x) = \frac{\gamma^\alpha}{\sigma_\alpha^3} f\left(\frac{|x-x^\alpha|}{\sigma_\alpha}\right) \quad (8)$$

where γ^α is the strength of the vortex element. The core function f is expressed by the following equation.

$$f(\varepsilon) = \frac{15}{8\pi(\varepsilon^2 + 1)^{7/2}} \quad (9)$$

2.4 Convection and change in strength of a vortex element

When the vorticity field is discretized into a set of N_v vortex elements, the gas velocity $u_g(x)$ is given by the following equation derived from Eqs. (7) and (8):

$$u_g(x) = -\frac{1}{4\pi} \sum_{\alpha=1}^{N_v} \frac{(x-x^\alpha) \times \gamma^\alpha}{|x-x^\alpha|^3} g\left(\frac{|x-x^\alpha|}{\sigma_\alpha}\right) + u_{g0} \quad (10)$$

where the function g is determined as:

$$g(\varepsilon) = 4\pi \int_0^\varepsilon f(\zeta) \zeta^2 d\zeta \quad (11)$$

The vortex element α convects with the gas velocity u_g given from Eq. (10). The Lagrangian approach is used for the calculation.

$$\frac{dx^\alpha}{dt} = u_g(x^\alpha) \tag{12}$$

Rewriting the vorticity equation, Eq. (6), in the Lagrangian co-ordinates, the equation is expressed as:

$$\frac{d\omega}{dt} = (\omega \cdot \nabla)u_g + \nu \nabla^2 \omega - \frac{1}{\rho_g} \nabla \times F_D \tag{13}$$

It is discovered from Eq. (13) that the vorticity of the vortex element varies with the lapse of time due to the change in the length of vortex element, the viscous diffusion, and the force exerted by the particles. The viscous diffusion is computed by applying a method to redistribute the vortex strength (Degond and Mas-Gallic, 1989). The particle effect is separately considered by the method explained in the next section. In this case, the substitution of Eqs. (8) and (10) into Eq. (13) yields the time rate of change in γ^α :

$$\begin{aligned} \frac{d\gamma^\alpha}{dt} = & \sum_{\beta=1}^{N_v} \frac{1}{\sigma^3} \left\{ -\frac{g(\zeta)}{\zeta^3} \gamma^\alpha \times \gamma^\beta + \frac{1}{\sigma^2} \left[-\frac{1}{\zeta} \frac{d}{d\zeta} \left(\frac{g(\zeta)}{\zeta^3} \right) \right] \right. \\ & \left. \times \left[\gamma^\alpha \cdot (x^\alpha - x^\beta) \right] \left[(x^\alpha - x^\beta) \times \gamma^\beta \right] \right\} \\ & + \frac{2\nu}{\sigma^2} \sum_{\beta=1}^{N_v} (\delta_\alpha \gamma^\beta - \delta_\beta \gamma^\alpha) \eta_\sigma(x^\alpha - x^\beta) \end{aligned} \tag{14}$$

where δ is the volume of vortex element, and $\zeta = |x^\alpha - x^\beta|/\sigma$. The last term on the right side of Eq. (14) corresponds to the viscous diffusion term, and $\eta_\sigma(x)$ is defined as:

$$\eta_\sigma(x) = \eta(|x|/\sigma)/\sigma^3 \tag{15}$$

where

$$\eta(\varepsilon) = -\frac{1}{\varepsilon} \frac{d}{d\varepsilon} f(\varepsilon) \tag{16}$$

2.5 Change in strength of vortex element due to particle

When substituting Eq. (6) into an equation, derived from the Reynolds transport theorem and Eq. (1), the time rate of change in the strength of vorticity γ in any volume is obtained:

$$\begin{aligned} \frac{D\gamma}{Dt} &= -\frac{1}{\rho_g} \int (\nabla \times F_D) dV \\ &= -\frac{1}{\rho_g} \int (n \times F_D) dS \end{aligned} \tag{17}$$

where n is the unit vector normal to the volume surface. The stretch-contraction term and the viscous diffusion term are omitted because they are already considered in Eq. (14).

2.6 Grid-based computation for strength of vorticity

In the three-dimensional vortex method proposed in a prior study (Uchiyama and Fukase, 2005), the entire flow field is resolved into hexahedral grids. A grid is shown in Fig. 1 (a). The time rate of change in the strength of vorticity γ , $\Delta\gamma/\Delta t$, in each grid is calculated from Eq. (17). If the F_D value is known on every surface of a grid, $\Delta\gamma/\Delta t$ is estimated from Eq. (17). For example, the x -component $\Delta\gamma_x/\Delta t$ is written as:

$$\frac{\Delta\gamma_x}{\Delta t} = -\frac{1}{\rho_g} [(F_{Dz}^B - F_{Dz}^A)\Delta S_y + (F_{Dy}^C - F_{Dy}^D)\Delta S_z] \tag{18}$$

where F_{Dz}^A is the F_{Dz} value on the surface A, and ΔS_y is the area of a surface normal to the y -axis, $\Delta x\Delta z$.

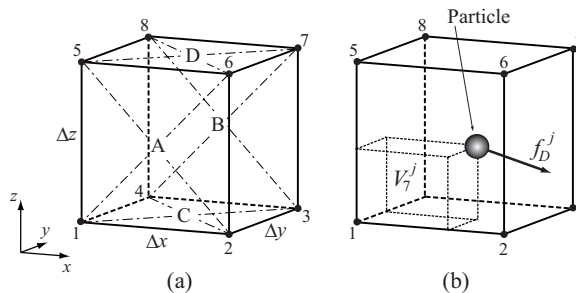


Figure 1: Computational grid employed in prior vortex method

When the number of vortex elements in a grid is n_v , the change in the strength for each vortex element during Δt is supposed to be $\Delta\gamma/n_v$. When there are no vortex

elements in the grid, a vortex element with a strength $\Delta\gamma$ is generated at the grid center.

The F_D value on a surface of a grid, such as F_{Dz}^A , is estimated by taking the average for the F_D values at four apexes of the surface. It is supposed that the number of particles in a grid is n_p and that the drag force f_D^j acts on the j th particle. The F_D value on an apex β , F_D^β , is given by the following equation:

$$F_D^\beta = \frac{1}{V} \sum_{j=1}^{n_p} \frac{V_\beta^j}{V} f_D^j \quad (\beta = 1, 2, \dots, 8) \quad (19)$$

where V is the grid volume $\Delta x \Delta y \Delta z$, and V_β^j is the volume concerning to the grid point β , as shown in Fig. 1 (b).

3 Grid-Free Simulation Method

3.1 Grid-free computation for strength of vorticity

Eight cubic cells, Cell 1 ~ Cell 8, are locally allocated around each particle, as depicted in Fig. 2. Their side length is L . The sides are parallel to the orthogonal coordinate axes. If the particle velocity relative to the gas is denoted by $v_p (=u_p - u_g)$, the drag force f_D acts in the direction of $-v_p$. The angle between f_D and the x -axis is postulated to be θ , while the angle between f_D and the z -axis is φ . Applying Eq. (19) to each cell, F_D acts only on the apex O on which the particle locates, and no forces act on the other apexes. Consequently, the components of F_D on the cell apexes are given by the following:

$$(F_{Dx}, F_{Dy}, F_{Dz}) = \begin{cases} (\xi_x, \xi_y, \xi_z) & \text{on apex } O \\ 0 & \text{on other apexes} \end{cases} \quad (20)$$

where

$$(\xi_x, \xi_y, \xi_z) = \frac{|f_D|}{L^3} (\cos \theta \sin \varphi, \sin \theta \sin \varphi, \cos \varphi) \quad (21)$$

With reference to the above-mentioned grid-based method, the F_D values on each surface of the eight cells are calculated by taking the average for the F_D values on the four apexes of the concerned surface. When the F_D value is computed on every surface by using Eq. (20), the change in the strength of vorticity in each cell, $\Delta\gamma$, is obtained from Eq. (17). The results are listed in Table 1.

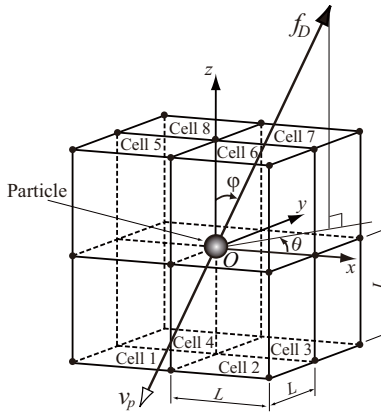


Figure 2: Eight cells around a particle

Table 1 Change of $\Delta\gamma$ in each cell due to particle

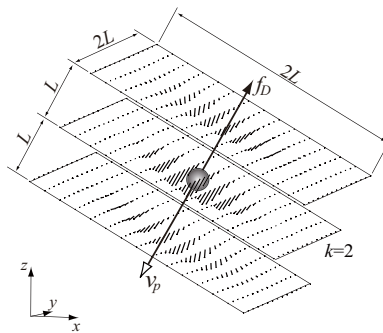
Cell	$(\Delta\gamma_x, \Delta\gamma_y, \Delta\gamma_z)$
1	$G(\xi_z - \xi_y, \xi_x - \xi_z, \xi_y - \xi_x)$
2	$G(\xi_z - \xi_y, \xi_x + \xi_z, -\xi_y - \xi_x)$
3	$G(-\xi_z - \xi_y, \xi_x + \xi_z, -\xi_y + \xi_x)$
4	$G(-\xi_z - \xi_y, \xi_x - \xi_z, \xi_y + \xi_x)$
5	$G(\xi_z + \xi_y, -\xi_x - \xi_z, \xi_y - \xi_x)$
6	$G(\xi_z + \xi_y, -\xi_x + \xi_z, -\xi_y - \xi_x)$
7	$G(-\xi_z + \xi_y, -\xi_x + \xi_z, -\xi_y + \xi_x)$
8	$G(-\xi_z + \xi_y, -\xi_x - \xi_z, \xi_y + \xi_x)$

$$G = -L^2\Delta t/4\rho_g$$

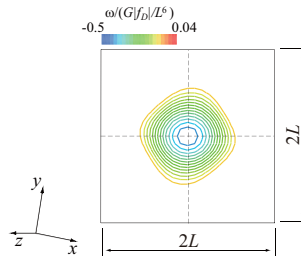
On the basis of the grid-based method proposed in a prior study (Uchiyama and Fukase, 2005), the change in the strength for each vortex element is supposed to be $\Delta\gamma/n_v$ when the number of vortex elements in the cell is n_v . A vortex element with a strength $\Delta\gamma$ is generated at the center of the cell when there are vortex elements in the cell.

It is postulated that one vortex element originates in each cell around a particle owing to the particle motion of $\theta=10^\circ$ and $\varphi=30^\circ$. The gas velocity distribution on three sections perpendicular to the particle motion is shown in Fig. 3 (a), where G and σ are set at $L^3/|f_D|$ and $L/2$ respectively. The velocity becomes higher with approaching the particle. It is axisymmetric with respect to the direction of the particle motion. A contracted flow occurs behind the particle, while an expanding

flow appears in front of the particle. Tanaka et al. (2007) also simulated these flows around a particle falling in air. Figure 3 (b) depicts the vorticity distribution on a section passing through the particle center. The vorticity takes its maximum value at the particle location, and the distribution is axisymmetric. These demonstrate that the proposed method simulates favorably the gas flow around a particle. It should be noted that the method is successfully applied for the particle motion with arbitrary values of θ and φ .



(a) Velocity vector



(b) Velocity contour

Figure 3: Gas flow field around a particle when $\theta=10^\circ$ and $\varphi=30^\circ$

The grid-based methods proposed by the author in prior studies (Uchiyama and Naruse, 2001; Uchiyama and Naruse, 2004; Uchiyama and Fukase, 2005) resolve the entire flow field into computational grids to calculate the change in the vorticity due to the particle in each grid. Therefore, they are partially based on the Eulerian method. The proposed grid-free method pays attention to each particle to calculate the vorticity field around the concerned particle, being the fully Lagrangian method. It promises to be usefully applied to simulate the flow in a region having complicated geometries. This is because the grid generation can be omitted in the simulation.

3.2 Numerical procedure

When the flow field at $t=t$ is known, the flow at $t=t + \Delta t$ is computed by the following procedure.

1. Calculate the position of vortex element from Eq. (12).
2. Calculate the change in strength of the vortex element due to the stretch-contraction and viscous diffusion from Eq. (14).
3. Calculate the particle motion from Eq. (3).
4. Arrange eight cubic cells around each particle as shown in Fig. 2.
5. Calculate the change in the strength of vorticity $\Delta\gamma$ by using Eq. (20) and Table 1.
6. Add $\Delta\gamma$ to the strength of the vortex elements in the concerned cell. When there are no vortex elements in the cell, generate a vortex element having the strength $\Delta\gamma$ at the center of the cell.
7. Calculate the gas velocity from Eq. (10).

4 Application to Free Falling of Solid Particles in Air

4.1 Simulation conditions

To demonstrate the validity and applicability of the proposed grid-free method, the behavior of solid particles falling in an unbounded air is simulated by the method. At the initial time $t^*=0$, spherical solid particles are arranged within a spherical region of diameter D in a quiescent air, as shown in Fig. 4. They are made to fall, and their fall induces the air flow around them, resulting in a gas-particle two-phase flow.

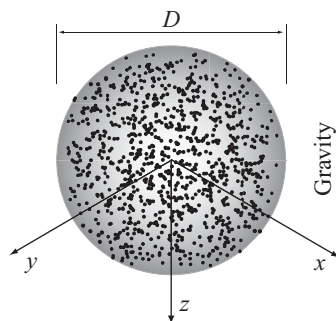


Figure 4: Initial arrangement of particles

The particle diameter d and density ρ_p are 1 mm and 7.7 kg/m^3 respectively, while the number of particles is 1000. The position at the commencement of the fall

($t^*=0$) is given by using random numbers. The diameter of spherical region D is set at $20d$. Accordingly, the particle volume fraction at $t^*=0$ is 0.125. The terminal velocity u_t calculated from Eq. (3) is 0.121 m/s. When the time scale of the induced air flow τ_g is assumed to be D/u_t , the Stokes number St , defined as the ratio of the particle response time $\tau_p (= \rho_p d^2 / 18 \rho_g \nu)$ to τ_g , is 1.44.

Since the air is quiescent at $t^*=0$, there are no vortex elements. The velocity u_{g0} in Eqs. (7) and (10) is zero, because the particles fall in an unbounded air. The time increment Δt is set at $u_t \Delta t / D = 6 \times 10^{-4}$, and the 2nd-order Adams-Bashforth method is applied to the Lagrangian calculation for the vortex element and the particle. The side length for the cubic cells arranged around each particle L is $0.5D$.

As a core radius σ in a vortex method corresponds to the half size of a computational grid in a Eulerian method, this simulation set σ at $L/2$. A simulation using smaller cells ($L=0.375D$) was also performed, but the result was not affected by the cells. Therefore, the cell size is found to be appropriate. It was possible to simulate by using much smaller cells of $L=0.25D$. However, the time advancement was extremely decelerated owing to the marked increment in the number of vortex elements.

The collisions between the particles are neglected. As the particle trajectory is computed by the Lagrangian method, it is not impossible to simulate the collisions.

4.2 Results and discussions

The time evolution for the particle distribution is shown in Fig. 5. The particle positions at eight time points from $t^*=0$ to $t^*=12.1$ are projected onto a vertical plane (x - z plane). The particles arranged in the half upper part ($z \geq 0$) and half lower one ($z < 0$) of the spherical region at $t^*=0$ are colored by red and blue respectively. The particles fall with destroying their initial arrangement, namely they tend to disperse in the horizontal direction. Most of the particles initially arranged in the half upper part sediment relatively toward the bottom for the particle-cluster, while the particles initially arranged in the half lower part rise relatively toward the top. These demonstrate that the particle behavior depends on the particle position at $t^*=0$ when $t^* \leq 4.84$. The particle dispersion in the horizontal (x) direction becomes markedly when $t^* \geq 4.84$. These particle motions are caused by the air flow induced by them, as explained later. It took 258 minutes for this simulation by using a personal computer (processor: 266 GHz \times 2, Memory: 4 GB).

Figure 6 shows the time evolution for the particle distribution projected onto a horizontal plane (x - y plane). Though the particles fall with dispersing in the lateral direction, they distribute within a circular region. Most of the particles initially

arranged in the half lower part, colored by blue, concentrate on the periphery of the circular region when $t^* \geq 3.03$. This is because the particles are whirled up by a vortex ring induced by them, as explained later. The concentration at the periphery is relaxed when $t^* \geq 7.26$, because the particles disperse in the horizontal direction with the passage of time.

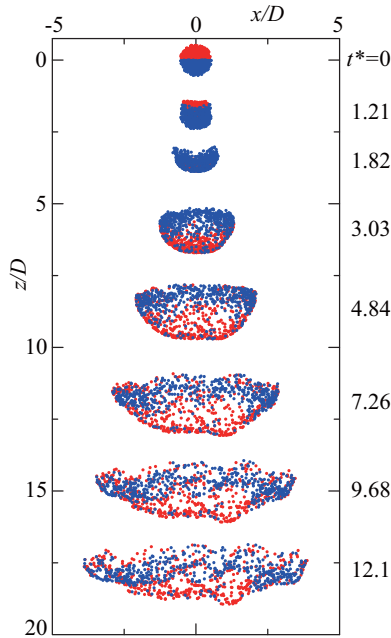


Figure 5: Time variation for distribution of particles on vertical section

The time evolution for the air velocity on a vertical plane (x - z plane) passing through the center of the particle-cluster ($x=y=0$) is shown in Fig. 7. To grasp easily the relation to the particles near the plane, the particles within a vertical slit region of $-0.03 \leq y/D \leq 0.03$ are also plotted. A vertically downward air flow occurs at the center of the particle-cluster when $t^* = 1.82$. The gravitational acceleration, which causes the particles to fall, induces the air flow through the drag force acting on the particles. Thus, the particles locating near the center of the particle-cluster sediment relatively in the downward direction. When $t^* \geq 1.82$, this downward air flow accelerates with the passage of time, and accordingly a pair of large-scale eddies occurs just above the falling particles. It corresponds to a vortex ring, being the wake of the particles, as explained later. The particles initially arranged in the half lower part of the spherical region are whirled up by the vortex ring, and therefore they concentrate on the periphery of the particles, as also seen in Fig. 6.

The particle distribution of such concave and thin layer types is caused by these sedimentation and whirl up. Since the particle falling velocity is higher than the convection velocity of the vortex ring, the space between the particles and the vortex ring increases with the passage of time. Consequently, the particles disperse more in the horizontal direction due to the air flow having a velocity in the $\pm x$ directions just below the vortex ring when $t^* \geq 4.84$.

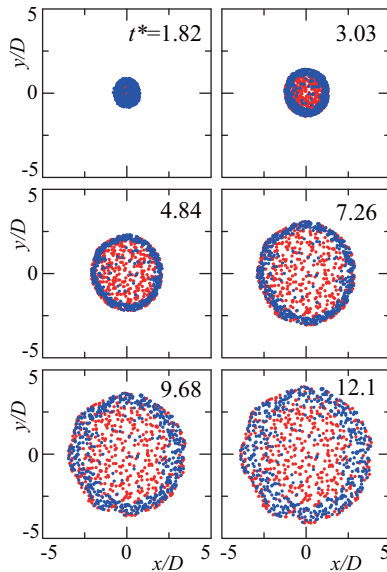


Figure 6: Time variation for distribution of particles on horizontal section

Experimental studies on a plane mixing layer (Wen et al., 1992) and a two-dimensional wake (Yang et al., 2000) reported that the particles of the Stokes number $St \approx 1$ are focused on thin layers, outlining the boundaries of the large-scale eddies. It was made clear by the author's grid-based vortex simulation (Uchiyama and Yagami, 2008; Uchiyama and Yagami, 2009) that such preferential distribution also appears when solid particles collide with a vortex ring. Considering that the St value of this simulation is 1.44, the simulated particle behavior corresponds to the above-mentioned preferential distribution. According to a two-dimensional simulation for the falling of particles of $St=1$ by Chen and Marshall (1999), an air flow is induced behind the particles, and a concave distribution of the particles occurs due to the wake flow. These support the validity of the present simulation.

The vorticity ω near the particles and the component in the vertical (z) direction ω_z distribute as shown in Fig. 8, where the iso-surfaces of $|\omega|D/u_t=1.65$ and $\omega_z D/u_t=\pm 0.165$ are presented. The particle distribution is also plotted. One can

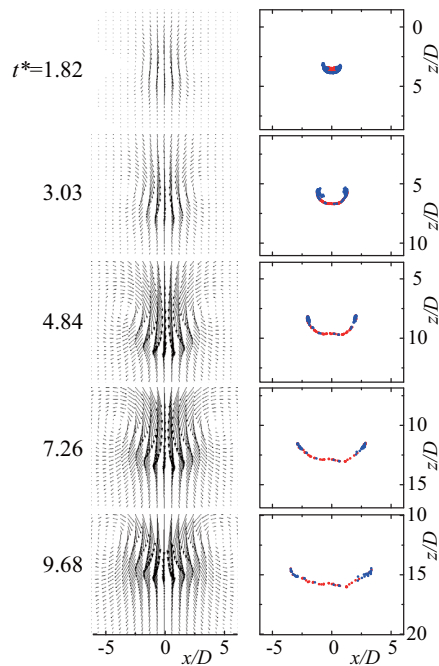


Figure 7: Air velocity and distribution of particles

observe the appearance of a vortex ring just above the particles when $t^* \geq 3.03$. Vortex tubes with positive and negative values of ω_z entangle around the vortex ring. The region, in which such complicated three-dimensional vortical flow exists, expands with the passage of time when $t^* \leq 9.68$.

The time evolution for the particle falling velocity \bar{u}_p is shown in Fig. 9, where \bar{u}_p is calculated by taking the average for the falling velocity of every particle. The velocity \bar{u}_p increases rapidly just after the commencement of the particle fall. It reaches the maximum value at $t^* = 1.57$. This is attributable to the fact that the particles are accelerated by the downward air flow induced by them. The velocity \bar{u}_p lessens monotonously at $t^* \geq 1.57$, and it tends towards the terminal velocity u_t . Because the distance between the vortex ring and the particles increases with the time evolution as seen in Figs. 7 and 8, and accordingly the effect of the vortex ring on the particles reduces.

In this simulation, the flow field is not bounded by solid walls. If the wall bounded flow is simulated, the non-slip condition on the wall is realized by representing the walls by some panels to apply existing grid-based vortex methods.

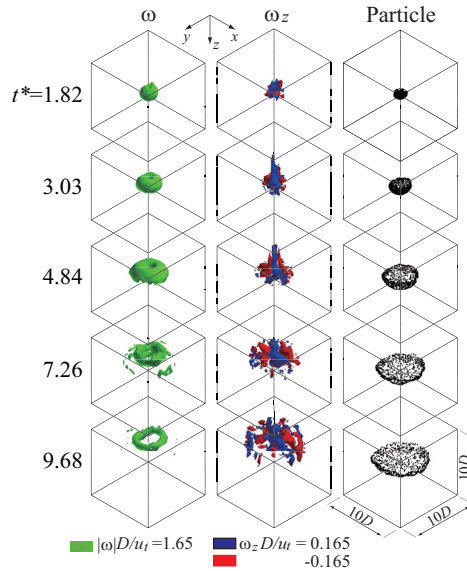


Figure 8: Air vorticity fields and distribution of particles

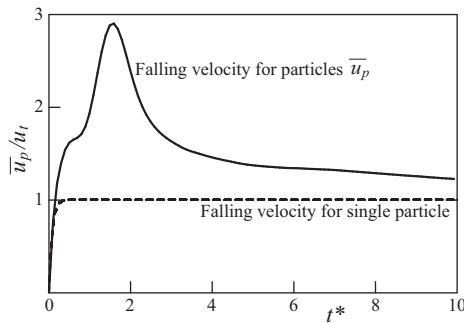


Figure 9: Time variation for falling velocity of particles

5 Conclusions

A three-dimensional grid-free simulation method for gas-particle two-phase flow is proposed. It is based on a vortex method. Eight cubic cells are locally allocated around each particle to consider the effect of the particle on the gas flow. In each cell, the change in the vorticity due to the particle motion is calculated, and it is considered by generating a vortex element or changing the strength of the existing vortex elements.

The grid-free method is also applied to simulate a free fall of small spherical solid particles. The particles, initially arranged within a spherical region in a quiescent air, are made to fall, and their fall induces the air flow around them, resulting in a gas-particle two-phase flow. The particles are accelerated by the induced downward air flow just after the commencement of their fall. After the acceleration, they are whirled up by a vortex ring produced around the downward air flow. These interactions between the particle motion and the air flow are favorably compared with the existing measured and simulated results. The validity of the proposed grid-free simulation method is successfully confirmed.

References

- Chen, H.; Marshall, J. S.,** (1999): A Lagrangian vorticity method for two-phase particulate flows with two-way phase coupling, *J. Comput. Phys.*, vol.148, pp.169-198.
- Cottet, G.-H.; Koumoutsakos, P. D.,** (2000): *Vortex Method: Theory and Practice*, Cambridge University Press.
- Crowe, C. T., et al.,** (1992): Multiphase flow with droplets and particles, CRC Press.
- Degond, P.; Mas-Gallic, S.,** (1989): The weighted particle method for convection-diffusion equations, *Math. Comput.*, vol.53, pp.485-507.
- Schiller, L.; Naumann, A. Z.,** (1933): Über die grundlegenden Berechnungen bei der Schwerkraftaufbereitung, *Z. Vereines Deutscher Inge.*, vol.77, pp.318-321.
- Tanaka, Y., et al.,** (2007), Measurement of the interaction between a single particle and a single burgers vortex, *Proc. 5th Joint ASME/JSME Fluid Eng. Conf.*, San Diego, FEDSM2007-37217, (on CD-ROM).
- Uchiyama, T.; Naruse, M.,** (2001): A numerical method for gas-solid two-phase free turbulent flow using a vortex method, *Powder Technol.*, vol.119, pp.206-214.
- Uchiyama, T.; Naruse, M.,** (2004): Numerical simulation for gas-particle two-phase free turbulent flow based on vortex in cell method, *Powder Technol.*, vol.142, pp.193-208.
- Uchiyama, T.; Fukase, A.,** (2005): Three-dimensional vortex method for gas-particle two-phase compound round jet, *Trans. ASME, J. Fluid Eng.*, vol.127, pp.32-40.
- Uchiyama, T.; Naruse, M.,** (2008): Two-dimensional grid-free simulation method for gas-particle two-phase flow based on vortex method, *Trans. JSME, Ser. B*, vo.74, pp.1324-1331.
- Uchiyama, T.; Yagami, H.,** (2008): Numerical simulation for the collision be-

tween a vortex ring and solid particles, *Powder Technol.*, vol.188, pp.73-80.

Uchiyama, T.; Yagami, H., (2009): Vortex simulation for non-axisymmetric collision of a vortex ring with solid particles, *Advanced Powder Technol.*, vol.20, pp.447-454.

Wen, F., et al., (1992): Particle dispersion by vortex structures in plane mixing layers, *Trans. ASME, J. Fluid Eng.*, vol.114, pp.657-666.

Winckelmans, G. S., (2004): Vortex Methods, *The Encyclopedia of Computational Mechanics*, vol.3, John Wiley & Sons.

Winckelmans, G. S.; Leonard, A., (1993): Contribution to vortex particle methods for the computation of three-dimensional incompressible unsteady flows, *J. Comput. Phys.*, vol.109, pp.247-273.

Yang, Y., et al., (2000): Experiments on particle dispersion in a plane wake, *Int. J. Multiphase Flow*, vol.26, pp.1583-1607.